

LETTER

Strong evidence of inter-layer optical phonons and low-temperature acoustic-phonon bunching in WS_2/WSe_2 hetero-structure


To cite this article: Hemanga J. Sarmah and D. Mohanta 2023 *EPL* **142** 46002

View the [article online](#) for updates and enhancements.

You may also like

- [Electron-doping Ruddlesden-Popper nickelate](#)
X. Chen, P. Jiang and Z. Zhong
- [Dipolar particles trapped in a cylindrical pore](#)
A. Mourad, H. Mohrbach and R. Messina
- [Spin-multiplexing phase-driven varifocal metalenses for multidimensional beam splitting and binary switching](#)
Yafeng Huang, Junwei Xu, Ximin Tian et al.

Strong evidence of inter-layer optical phonons and low-temperature acoustic-phonon bunching in WS₂/WSe₂ hetero-structure

HEMANGA J. SARMAH^{1,2} and D. MOHANTA^{1(a)} 

¹ Nanoscience and Soft-Matter Laboratory, Department of Physics, Tezpur University - PO: Napaam, Tezpur-784028, Assam, India

² Department of Physics - Morigaon College - Morigaon-782105, Assam, India

received 15 November 2022; accepted in final form 18 April 2023
published online 25 May 2023

Abstract – The nature of inter-layer optical phonons observed in the WS₂/WSe₂ hetero-structure is being reported in this work. Additionally, phonon bunching between $3E_{2g}^2$ modes of both WS₂ and WSe₂ can be ascertained in the acoustic region. The second-order bunching factor, $g^{(2)}$, is seen to improve sharply upon reduction of temperature, below a critical temperature. Moreover, the integral intensity of the peaks increases almost exponentially with the applied power of the laser source. To a good approximation, the phonon frequency corresponding to most of the Raman active modes varies linearly with altered temperature (78–300 K). However, the $A_{1g}+A_{1g}^*$ mixed mode located at $\sim 661\text{ cm}^{-1}$ exhibits a non-linear temperature dependence over the working range of temperature. Prevailing phonon bunching aspects of the phonon replica discussed in terms of bunching factor, frequency correlation parameter, etc., are highlighted based on acquired low-temperature Raman data and theoretical analogy.

Copyright © 2023 EPLA

Unfailing stories of graphene and its derivatives have paved the path for a variety of two-dimensional (2D) materials, which in fact accelerated fundamental and applied research. While the research community is eager to witness the unprecedented benefits of these layered systems in the near future, major implications are expected to rely on spintronics, energy harvesting, valley transport and quantum transport [1–3]. Of recent interest, layered transition metal mono- (TMMs) and di-chalcogenides (TMDs) have proven potential to act as new testbeds for studying vibrational spectroscopy, exciton physics, charged exciton dynamics and inter-valley transitions, in addition to relevance in solid lubrication, photo sensing and photocatalytic activities [4–6]. In this work, the focus is on the effect of temperature dependence on different phonon modes in WS₂/WSe₂ hetero-structures.

Quantum effects in spatially confined systems are now at the forefront owing to their incredibly high demand in the field of quantum transport [7], quantum point contacts (QPCs) and linkages [8], dissipative quantum engineering [9] as well as quantum statistics [10]. In exotic statistics, the correlation factors are critically examined to

probe the information being exchanged between the two non-interacting and distinguishable particles [11]. Undeniably, bunching, and anti-bunching of photons form the basis behind any such influence [12]. Temporal correlation of photons causing bunching/anti-bunching effects has been rigorously studied after initial experiments laid down by Brown and Twiss [13]. Retaining the equally important bosonic criterion exhibited by phonons, it may also dictate crowding under suitable environment. Originally, Okuyama *et al.* hypothesized infrequent phonon bunching in quantum dots (QDs) [14] and later elaborated by Guan *et al.* [15] as regards explaining phonon anti-bunching in coupled non-linear micro/nano mechanical resonators in the light of a theoretical framework. Recently, Cayla *et al.* has provided experimental evidence of bunching of phonons in the case of the boson gas [16]. In another study, vibrational features of WSe₂/WS₂ hetero-structure have been reported [17]. However, the present work highlights interlayer phonons and temperature-dependent acoustic-phonon bunching spectral features divulged in nanoscale WS₂/WSe₂ hetero-structures formed by virtue of stacking-restacking attempt.

Morphological evidence of the exfoliation followed by stacking of WS₂/WSe₂ hetero-structures can be visualized

^(a)E-mail: best@tezu.ernet.in (corresponding author)

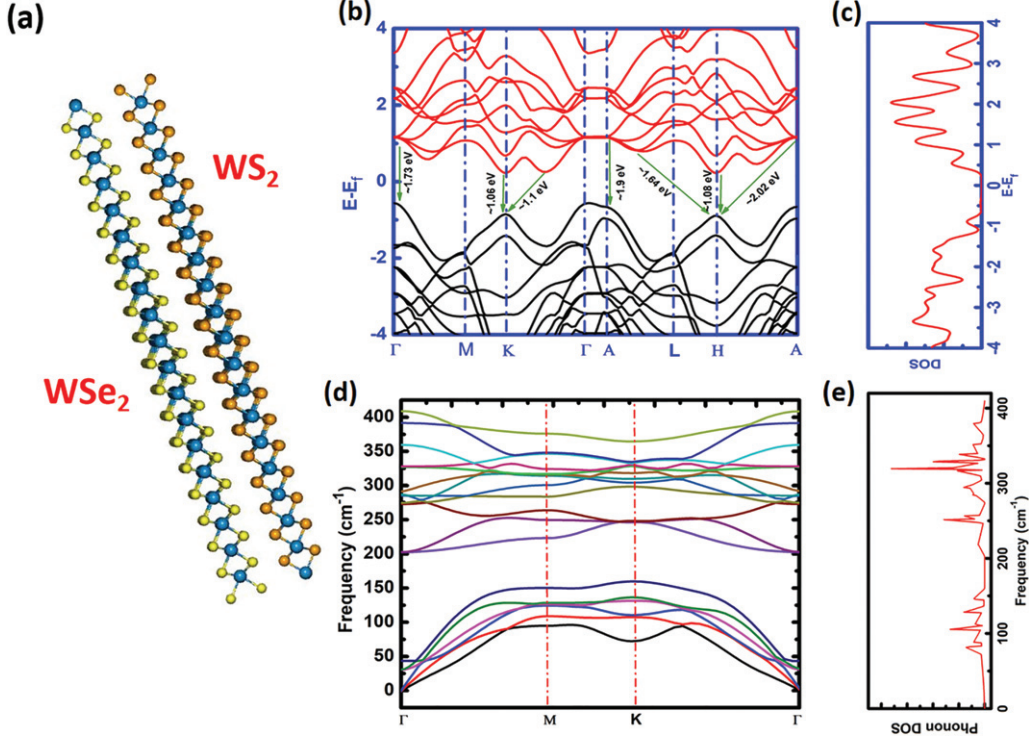


Fig. 1: (a) A schematic representation of the WS₂/WSe₂ hetero-structure derived using Quantum Espresso. (b) Electronic band structure of the WS₂/WSe₂ hetero-structure, (c) electronic density of states profile, (d) phonon dispersion features for theoretically obtained 18 modes. Note: two different regions for acoustic and optical phonon modes maybe seen. (e) Phonon density of states.

from the high-resolution transmission electron micrograph (HRTEM) depicted in fig. S1 of the Supplementary Material [SupplementaryMaterial.pdf](#) (SM). Apparently, in the bilayer system with one layer (I: WS₂) lying beneath the other (II: WSe₂), with respective interatomic spacings ~ 0.266 nm and ~ 0.284 nm corresponding to (100) planes. A clear indication of the overlapped segments of the sheets with a twist angle of approximately 60° can be found. To be noted, formation of WS₂/WSe₂ hetero-structures in 0° and 60° twist angles has been reported earlier via vapor growth method. Feasible in the low-temperature region, the later stacking angle was believed to be favorable thermodynamically [18]. In addition, the TMDs hetero-structure in the 60° twist angle exhibits the lowest values of band gap and inter-layer distance [19]. Moreover, the selective area electron diffraction (SAED) pattern, captured in *region A* of layer-I portrays assembly of bright spots in hexagonal configuration, and that in *region B* of stacked layers (I and II), highlighting a diffused ring pattern. Furthermore, X-ray photo-electron spectroscopy (XPS) analysis was employed to substantiate the development of WS₂/WSe₂ hetero-structure, presented in the SM (fig. S2).

A schematic illustration of WS₂/WSe₂ hetero-structure is depicted in fig. 1(a). Calculations have been conducted employing first-principle-based density functional theory (DFT) and using Quantum Espresso[®] package (QE) [20].

The projector augmented wave (PAW) pseudopotential was considered to describe the electron-core interaction process and the generalized gradient approximation (GGA) of Perdew-Burke-Ernzerhof (PBE) to form the exchange correlation potential [21]. A grid of \mathbf{K} point sampling $9 \times 9 \times 1$ is taken based on the Monkhorst-Pack scheme to perform the Brillouin zone interactions with a cut-off energy of 650 eV. Again, the supercell structure has been optimized in all directions till the energy and the force per atom are less than 1.0×10^{-8} eV and 0.01 eV/Å, respectively. The predicted electronic band structure of WS₂/WSe₂ hetero-structure can be found from fig. 1(b). Apparently, the WS₂/WSe₂ hetero-structure exhibits a semiconducting direct band gap of ~ 1.08 eV, positioned at the \mathbf{K} point of the reciprocal lattice. Besides that, the finite gaps namely, ~ 1.08 eV, ~ 1.73 eV and ~ 1.9 eV could be traced for \mathbf{H} , $\mathbf{\Gamma}$ and \mathbf{A} valley points. Additionally, momentum-conserved, phonon-assisted indirect band gaps amounting to 2.02 eV, 1.1 eV and 1.64 eV can be visualized in the electronic structure. In pure form, the WS₂ and WSe₂ would possess a band gap of ~ 2 eV and ~ 1.73 eV, respectively; and thus, unusual gaps of ~ 1.1 eV or 1.64 eV possibly represent intermediary interlayer excitonic states. The existence of interlayer excitons has already been discussed in the literature [22]. The estimated values are slightly higher compared to the reported ones, *i.e.*, ~ 1.5 eV. To obtain a better picture, the

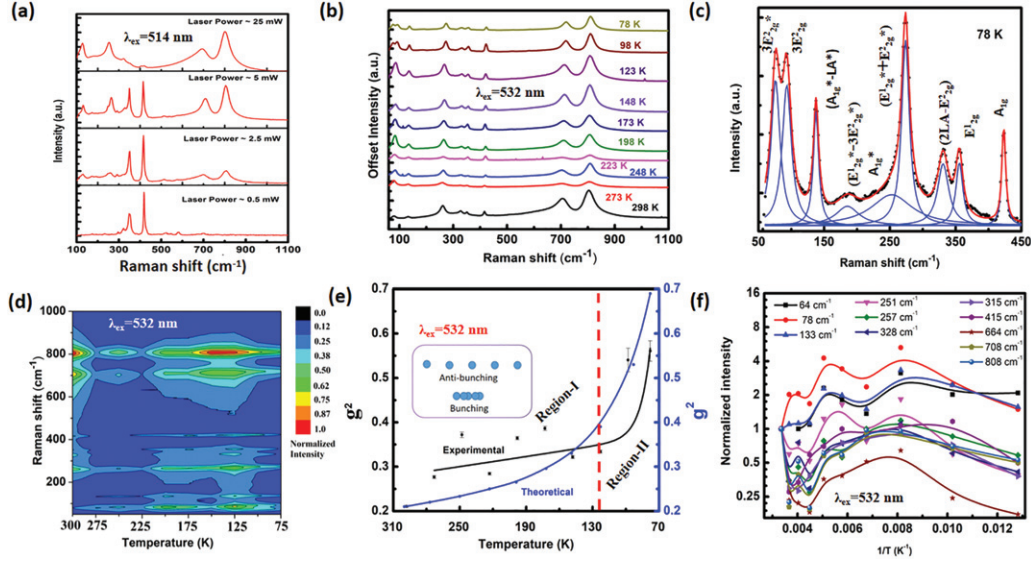


Fig. 2: (a) Power-dependent Raman spectra of the WS_2/WSe_2 hetero-structure. Note: in higher laser power (p_i), modes related to the WSe_2 became more prominent compared to that of WS_2 . (b) Temperature-dependent Raman spectra of the WS_2/WSe_2 hetero-structure. (c) Deconvoluted Raman spectra at 78 K. (d) A contour plot of the Raman active modes with temperature. (e) Second-order correlation factor ($g^{(2)}$): a comparative view between theory and experiment. Note: here two different regions can be witnessed. Region-I (above 123 K): $g^{(2)}$ value improves slowly with lowering temperature. Region-II (below 123 K): $g^{(2)}$ value rises steeply with declining temperature. A schematic representation of bunching and anti-bunching is depicted in the inset, and (f) non-linear temperature dependency of different Raman active modes in reference to room temperature characteristics.

density of states (DOS), $D(\varepsilon)$ calculations for the hetero-layer WS_2/WSe_2 are shown in fig. 1(c). Although a finite tailing gap of 1.06 eV has been predicted from the DOS data, prominent transitions among the extended states could be suspected above the exciton energies.

We could envision possible phonon modes as well as phonon dispersion curves by implementing the density functional perturbation theory featuring calculations based on the QE package and considering $3 \times 3 \times 1$ supercell as the test sample. About 18 phononic modes, including mixed and collective ones can be ascertained. Phonon frequencies ascribed to distinctly different modes and within the Brillouin zone were estimated and presented in table S1 in the SM. The dispersion curves, which characterize variation of phonon frequency, ω with the phonon wave vector, \mathbf{q} are depicted in fig. 1(d). The phonon density of state, D_q , is also calculated and presented in fig. 1(e). Ideally, the group velocity of the phonon package is defined as

$$v_g = \frac{d\omega}{dq}, \quad (1)$$

with \mathbf{q} being the wave vector in reciprocal space. Anomalous variation of the group velocity for the predicted acoustic modes can be found in the SM. Note the maximum attainable group velocity (~ 600 a.u.) tending to drop to its minimal value at the M point in the reciprocal lattice.

To explore vibrational features experimentally, temperature-dependent (78–300 K) resonant Raman spectroscopy has been employed for the WS_2/WSe_2

hetero-structure, using a 532 nm line of He-Ne laser as the excitation source. Also, power-dependent spectra have been obtained by employing 514 nm line of Ar^+ ion laser (0–25 mW, 300 K), shown in fig. 2(a). Apparently, the spectra reveal Raman active modes appearing at 131 cm^{-1} , 251 cm^{-1} , 257 cm^{-1} , 333 cm^{-1} , 350 cm^{-1} , 418 cm^{-1} , 664 cm^{-1} , 707 cm^{-1} and 807 cm^{-1} . Numerous comparatives and analogous phononic modes as predicted from the theoretical calculations are listed in table S1, in the SM. Also, these peaks are quite evident in the low-temperature regime, as substantiated from the fig. 2(b). Besides, distinct modes have been obtained from the independent WS_2 and WSe_2 layers. For instance, the peaks positioned at $\sim 332 \text{ cm}^{-1}$, 350 cm^{-1} , 418 cm^{-1} and 707 cm^{-1} correspond to the associated Raman active modes signifying $(2LA-E_{2g}^2)$, E_{2g}^1 , A_{1g} , and $4LA$ in the WS_2 system. On the other hand, the peaks located at $\sim 131 \text{ cm}^{-1}$, 185 cm^{-1} , 231 cm^{-1} and 273 cm^{-1} could emerge due to the mixed modes of $(A_{1g}^* - LA^*)$, $(E_{2g}^{1*} - 3E_{2g}^{2*})$, $(2LA^* - E_{2g}^{2*})$ and $(E_{2g}^{1*} + E_{2g}^{2*})$. Also, two independent modes located at $\sim 252 \text{ cm}^{-1}$ and 257 cm^{-1} may be assigned to E_{2g}^{1*} and A_{1g}^* Raman active modes, evident in the WSe_2 system [23]. For clarity, the deconvoluted spectral feature for the lowest temperature (78 K) case is depicted in fig. 2(c). To avoid technical ambiguity, Raman modes of the WSe_2 are designated with an “*” mark. Interestingly, the presence of most prominent mode at, $\sim 808 \text{ cm}^{-1}$ (φ) in all the cases is recognized as the fourth harmonic of mode 7, which appears at high laser power (and at low temperature discussed in the

subsequent section, for ~ 148 K) and possibly because of higher phonon population density (table S1). Astoundingly, exciting at a higher laser power of ~ 25 mW reveals an asymmetrically broadened peak found at ~ 707 cm^{-1} ($4LA$ of WS_2) which upon deconvolution, offered a shoulder peak located at 661 cm^{-1} . This unusual, mixed mode ($A_{1g} + A_{1g}^*$) was believed to have arisen from the heterolayers, signifying interlayer phonons excited in the WS_2/WSe_2 system. Arising interlayer phonon in higher laser power indicates that a significant amount of excitation energy is crucial for their excitation and sustenance. Knowing that, Raman intensity is hugely dependent on the phonon density trend with the phonons obeying the Bose-Einstein (BE) statistics stated as

$$n_{ph} = \frac{n_o}{\exp\left(\frac{\hbar\omega_{ph}}{k_B T}\right) - 1}, \quad (2)$$

where $k_B T$ is the thermal energy at the absolute temperature, T and k_B as Boltzmann's constant. Not surprisingly, an increase in laser power could excite more and more phonons and consequently, populate the phonon density of states, D_q featuring intense Raman active modes of E_{2g}^{1*} (A_{1g}^*), $2LA$, and φ with increasing laser power (fig. S3, (SM)). The intensity variation follows a nearly exponential dependence with the laser power, p_l and is given by

$$n_{ph} = \chi \exp(A p_l), \quad (3)$$

where A is a constant and χ as the pre-exponential factor.

The origins of low-lying peaks located at ~ 79.9 cm^{-1} and ~ 64 cm^{-1} can be ascribed to acoustic phonons as predicted from the dispersion curves and depicted in fig. 2(d). Compared with the usual modes of WS_2 and WSe_2 systems they were identified as third harmonic modes, $3E_{2g}^{2*}$ and $3E_{2g}^{2*}$. To be mentioned, the $3E_{2g}^{2*}$ peak is less prominent as compared to the $3E_{2g}^{2*}$ mode at room temperature ($I_{3E_{2g}^{2*}} < I_{3E_{2g}^{2*}}$). At lower temperature, however, the peak $3E_{2g}^{2*}$ becomes significant ($I_{3E_{2g}^{2*}} \approx I_{3E_{2g}^{2*}}$) and tending to shift towards $3E_{2g}^{2*}$ mode, offering an asymmetry. Moreover, distinct variation in the peak positions with increasing temperature can be witnessed in the contour plot, depicted in fig. 2(d). Interestingly, the signature of phonon bunching can be well resolved at lowered temperatures owing to the superposition of phonon wavefunctions while taking advantage of reduced thermal noise. Previous reports on photon bunching can help determine the strengths of the phonon bunching expressed in terms of the steady state density (ρ), creation (b^\dagger) and annihilation operators (b) [14–16]:

$$g^{(2)} = \frac{\langle b^\dagger b^\dagger b b \rho \rangle}{\langle b^\dagger b \rho \rangle^2}. \quad (4)$$

Here, the factor $g^{(2)}$ represents the probability of finding both the phonons (from independent systems) simultaneously with respect to the probability of finding each

phonons separately. Using the experimental data, the $g^{(2)}$ values were determined considering the ratio of square of the overlapping area of both the peaks to the product of integral intensities of those peaks. Referring to the room temperature (300 K) case, the $g^{(2)}$ value is estimated to be as low as ~ 0.21 , which would signify negligible phonon bunching. In fact, an enhanced possibility of phonon bunching effect can be anticipated at lower temperatures, offering an augmented $g^{(2)}$ value of ~ 0.56 . With a bosonic field in place, the superposition of two phonon wave functions can be suspected due to suppressed thermal agitation. Prior to this work, Gaun *et al.*, have showed the phonon bunching effect theoretically, analogous to the photon bunching effect [15]. Implementing the mechanical resonator model, the Hamiltonian can be stated in terms of strength of the mechanical resonator in energy unit (J), external perturbation in energy unit (F) and non-linearity terms (U) as [15]

$$H = \Delta b_1^\dagger b_1 + \Delta b_2^\dagger b_2 + J(b_1^\dagger b_2 + b_2^\dagger b_1) + F(b_1^\dagger + b_1) + U b_2^{2\dagger} b_2^2. \quad (5)$$

Here, Δ stands for frequency equivalent energy difference between two phonons, and b_i^\dagger (or b_i) is the creation (or annihilator) operator for the i -th resonator. The simplified form of the second-order correlation factor $g^{(2)}$ is formulated as [15]

$$g^{(2)} = \frac{2\rho_{66}}{(\rho_{44})^2}. \quad (6)$$

The ρ_{66} and ρ_{44} terms are presented in the SM.

Keeping in mind the best fitted trend between the theory and experiment, the non-linear factor U is estimated as $\sim 5 \times 10^{-4}$. At the same time, considering other parameters namely, $J = 11$ meV and $F = 2.1$ eV, an appropriate trend for $g^{(2)}$ is expected, shown in fig. 2(e). Here, $T_o = 123$ K is the equivalent phonon temperature of average energy between the two modes, offering bunching phenomena in two separate regions. Noticeably, a slow yet linearly growing trend was quite relevant over the temperature range 298–123 K, prior to witnessing sharp rising feature at relatively lower temperatures (123–77 K). The experimental and theoretical curves would meet in the cross-over region at ~ 150 K.

The increasing trend of the $g^{(2)}$ value in the low temperature implies that, in the absence of excessive thermal disturbances, the acoustic in-plane modes for both the systems (WS_2 and WSe_2) could be supported independently, along with the superposition of acoustic in-plane phonons. Apart from these, optical out-of-plane phonon modes were seen to be positioned at ~ 257 cm^{-1} (WSe_2) and 418 cm^{-1} (WS_2) self-reliantly at all temperatures.

As can be found in fig. 2(d), the interlayer phonon peak, ($A_{1g} + A_{1g}^*$) appearing at ~ 661 cm^{-1} reveals a noticeable widening with varying temperature. To probe the dependency of the interlayer phonons with its original modes

A_{1g} and A_{1g}^* , let us introduce a frequency correlation parameter:

$$f_\omega = \frac{\omega(A_{1g} + A_{1g}^*)}{\omega(A_{1g}) + \omega(A_{1g}^*)}. \quad (7)$$

The f_ω value could attain to the tune of 0.98 at 300 K, which slightly drops very sharply to a value of 0.92 at 250 K, followed by steady non-linear behavior with the lowering of temperature. Alteration of f_ω with varying temperature is also shown in the SM (fig. S6).

Exhibiting linear temperature dependence over scattered data (not shown), the shifting of the representative modes, E_{2g}^1 , A_{1g} , E_{2g}^{1*} , A_{1g}^* can be brought to a general expression,

$$\omega(T) = \omega(o) + \beta T, \quad (8)$$

where $\omega(o)$ is the phonon frequency at absolute zero temperature, β is the thermal coefficient of vibration. It is worth mentioning here that a noticeable temperature-dependent shifting of the vibrational modes has already been reported for the ReSe₂ system [24].

In addition to frequency shifting of the Raman active modes, anomalous intensity variation may be noted as regards different temperature conditions, with significant intensity drops for cases of 273 K and 223 K (fig. 2(b)). This is substantiated by the non-linear oscillating trend in the intensity *vs.* inverse temperature plot (fig. 2(f)). This non-linear behavior is suspected due to adequate interaction between phonons in heterolayers. Considering $x = \frac{\hbar\omega_{ph}}{k_B T}$, the modified expression can be stated as

$$n_{ph} = \frac{n_o}{\exp(a + bx + cx^2) - 1}. \quad (9)$$

Only for optical modes, $\hbar\omega_{ph} \gg k_B T$ so that the above relation reduces to

$$\log\left(\frac{n_{ph}}{n_o}\right) = -(a + bx + cx^2), \quad (10)$$

where a , b , and c are constants with $c \neq 0$ representing non-linear dependency of the phonon intensity of the system. To be mentioned, prior to this work, anharmonic Raman intensity due to phonon-phonon interaction was reported elsewhere [25]. Despite obeying non-linear behavior, acoustic and optic modes would manifest markedly. Normalized intensity of the first kind is always greater than unity at low temperature, while the second one is lesser than unity (except for the $\sim 251 \text{ cm}^{-1}$ peak). Interestingly, optic mode intensities improve upon increasing temperature, from 78 K up to 123 K. A further increase in the temperature results in the declining of the peak intensity up to 248 K, followed by an increasing trend thereafter. Alteration in the peak intensities of different modes could be easily witnessed both from the contour plot and comprehensive 3D plots, presented in fig. 2(d) and fig. S4 (SM), respectively.

In summary, the evidence of interlayer phonons could be adjudged in the WS₂/WSe₂ hetero-structure, which

arises due to the combinational effect of phononic features. Additionally, phonon bunching is also witnessed between 16530 cm^{-1} $3E_{2g}^2$ modes of both material species. The second-order bunching factor is seen to be improved upon reduction of temperature, experimentally as well as theoretically. Moreover, the intensity of the peaks increases almost exponentially with the applied power of the laser source. With varying temperature, a linear temperature dependence of the phonon frequency has been predicted, except the $(A_{1g} + A_{1g}^*)$ mode, which initially drops exponentially then tending to improve linearly. Apart from these, the scope of theoretical treatments as regards phonon modes and dispersion relation has also been examined and elaborated.

The authors acknowledge IUAC, New Delhi (UFR-62312) for the financial support. The facility extended through UGC-SAP DRS II of Department of Physics, Tezpur University is gratefully acknowledged. IASST-Guwahati and NERIST, Jorhat are noted for HRTEM and XPS facilities, respectively. Solid State Physics Division, BARC, Mumbai and SAIC, TU are acknowledged for low and room temperature Raman facilities, operating at 532 nm and 514 nm excitation, respectively. Special thanks to Dr. R. RAO, for her help in the Raman studies and to Dr. S. K. BEHERA for some useful discussion and support in theoretical calculations.

Data availability statement: The data that support the findings of this study are available upon reasonable request from the authors.

REFERENCES

- [1] MANZELI S., OVCHINNIKOV D., PASQUIER D., YAZYEV O. V. and KIS A., *Nat. Rev. Mater.*, **2** (2017) 1.
- [2] CHOI W., CHOUDHARY N., HAN G. H., PARK J., AKINWANDE D. and LEE Y. H., *Mater. Today*, **20** (2017) 116.
- [3] OU H. *et al.*, *Phys. Rev. Mater.*, **6** (2022) 064005.
- [4] WANG S. W. *et al.*, *ACS Nano*, **11** (2017) 8768.
- [5] KOLOBOV A. V. and TOMINAGA J. (Editors), *Two Dimensional Transition Metal Dichalcogenides*, Springer Series in Material Science, Vol. **239** (Springer) 2016.
- [6] REN W., CHEN J. and ZHANG G., *Appl. Phys. Lett.*, **121** (2022) 140501.
- [7] KUMAR S., *J. Phys: Condens. Matter*, **31** (2019) 200301.
- [8] WANG X., MIRANOWICZ A., LI H. R. and NORI F., *Phys. Rev. B*, **95** (2017) 205415.
- [9] ROSSLER C. *et al.*, *New J. Phys.*, **13** (2011) 113006.
- [10] WU Y. S., *Phys. Rev. Lett.*, **52** (1984) 2103.
- [11] MANNING A. G., *Foundation experiments in quantum atom optics with ultracold metastable helium*, PhD Thesis, Australian National University (2014).
- [12] MICHLER P. *et al.*, *Nature*, **406** (2000) 968.

- [13] BROWN R. H. and TWISS R. Q., *Nature*, **177** (1956) 27.
- [14] OKUYAMA R., ETO M. and BRANDES T., *New J. Phys.*, **15** (2013) 083032.
- [15] GUAN S., BOWEN W. P., LIU C. and DUAN Z., *EPL*, **119** (2017) 58001.
- [16] CAYLA H. *et al.*, *Phys. Rev. Lett.*, **125** (2020) 165301.
- [17] CHUANG H. J. *et al.*, *ACS Nano*, **16** (2022) 16260.
- [18] WU L. *et al.*, *Nano Res.*, **14** (2021) 2215.
- [19] WANG S. *et al.*, *Adv. Mater.*, **33** (2021) 2005735.
- [20] GIANNOZZI P. *et al.*, *J. Phys.: Condens. Matter*, **21** (2009) 395502.
- [21] PERDEW J. P., BURKE K. and ERNZERHOF M., *Phys. Rev. Lett.*, **77** (1996) 3865.
- [22] WANG K. *et al.*, *ACS Nano*, **10** (2016) 6612.
- [23] BHATT S. V., DESHPANDE M. P., SATHE V., RAO R. and CHAKI S. H., *J. Raman Spectrosc.*, **45** (2014) 971.
- [24] JIANG S. *et al.*, *Nanotechnology*, **29** (2018) 204003.
- [25] SAMANTA K., BHATTACHARYA P. and KATIYAR R. S., *Phys. Rev. B*, **75** (2007) 035208.